2003-01-1489

Vibration Characteristics of Cardboard Inserts in Shells

Martin G. Foulkes and James P. De Clerck
General Motors Corporation

Rajendra Singh
The Ohio State University

ABSTRACT

A study has been conducted to determine the noise and vibration effect of inserting a cardboard liner into a thin, circular cross-sectioned, cylindrical shell. The relevance of such a study is to improve the understanding of the effects when a cardboard liner is used in a propeller shaft for noise and vibration control purposes. It is found from the study that the liner adds significant modal stiffness, while an increase in modal mass is also observed for a particular shell type of mode. Further, the study has shown that the additional modal damping provided by the liner is not appropriately modeled by Coulomb friction damping, a damping model often intuitively associated with cardboard materials. Rather, the damping is best modeled as proportional viscous damping.

INTRODUCTION

Propeller shaft resonant vibration can be a noise and vibration control issue in the operation of motor vehicles. While certain characteristics of noise and vibration originating from the engine can be pleasing to an occupant, the drive line components are expected to be transparent. Therefore, various treatments have been developed to reduce the resonant behavior in propeller shafts. These treatments exist in forms ranging from press-fit cardboard to foam injected into the shaft in a liquid state and expanded to fit during a curing process. While many companies apply these treatments to the shaft, the physical phenomena behind the vibration attenuation are not fully known. Further knowledge of the attenuation mechanism is required to design and optimize the treatments in a more efficient manner during the product development process.

The paper presents the results of a study conducted to address the physical phenomenon behind a press fit cardboard liner used to attenuate resonant vibration in a circular cross-sectioned, thin-walled, cylindrical shell. Experimentally determined frequency response functions (FRFs) and curve-fitted modal parameters of a thin cylinder are compared to determine the mass, stiffness, and damping effects when the cardboard liner is applied to the interior wall of the shell. To aid in identifying the modal changes in the system, a portion of thin shell theory is used to properly characterize the mode types in the shell system. Furthermore, the appropriate damping model for the cardboard liner is determined by two different approaches. First, inspection of the acceleration response decay envelopes in the time domain is used to evaluate the presence of Coulomb friction damping; this damping model is often intuitively associated with a cardboard treatment. Second, observations from the damping matrices constructed using experimentally curve-fitted complex natural frequencies and mode shapes are presented in order to determine if the appropriate damping model is in fact viscous or some other form of damping.

MODAL EFFECTS OF THE LINER

A common way of determining the mass, stiffness, and damping changes in a system is to compare FRFs when the change is made to the system. An increase in frequency for a particular mode usually implies an increase in modal stiffness of the system, while a decrease in frequency can be associated with an increase in modal mass. A reduction and widening of the resonant peak usually implies an increase in modal damping. To be able to track the frequency changes of each mode, proper identification of the mode shape is required. To aid in this task, thin shell theory is employed to characterize the spatial behavior of each mode in a circular cross-sectioned cylindrical shell.

THIN SHELL THEORY

A number of theories for the vibration behavior of circular cross-sectioned cylindrical shells are available in the literature. In particular, Ref [1] presents a comprehensive list of the theories and compares the published results for many different cases. The determination of mode shapes for a free-free boundary condition is reproduced here. Certain limiting cases are assumed when applying thin shell theory. They are:

1. Constant wall thickness, small deflections, and the middle surface of the shell deforms without stretching.
2. Effects dealing with initial stress, shear deformation, and rotary inertia are excluded.
3. The material is considered isotropic and homogeneous.

The geometric variables for the shell under consideration are shown in figure 1. The displacement functions u, v, and w on the surface of the shell are determined from equations (1)—(3):

$$u = \sum_m A_m X'(x)\cos(n\theta)\cos(\omega t) \quad (1)$$

$$v = \sum_m B_m X(x)\sin(n\theta)\cos(\omega t) \quad (2)$$

$$w = \sum_m C_m X(x)\cos(n\theta)\cos(\omega t) \quad (3)$$

Where, A_m, B_m, and C_m are amplitude coefficients, m is the number of circumferential nodal circles, and n is the number of circumferential nodal waves. $[\bullet]'$ denotes the first derivative. The corresponding beam function, *X*, in (1)—(3) for a free-free boundary condition is given in (4) as:

$$X_m = \cosh(\lambda_m s) + \cos(\lambda_m s) - \alpha_m[\sinh(\lambda_m s) + \sin(\lambda_m s)]$$
for *m=1,2,3,…* (4a)

$$X_R = 1 \quad (4b)$$

$$X_L = \frac{x}{l} + \frac{1}{2} \quad (4c)$$

Where $s = x/R$, $\lambda_m = R\varepsilon_m/l$, ε_m and α_m are tabulated in Ref [1]. Equations 4(b) and (4c) are special cases of in-extensional mode shapes: the Rayleigh type modes and the Love type modes, respectively. Figure 2 displays the mode shape for the first bending mode or an (m,n) value of (1,1). The mode shapes for other modes are shown in Figure 9 in the appendix.

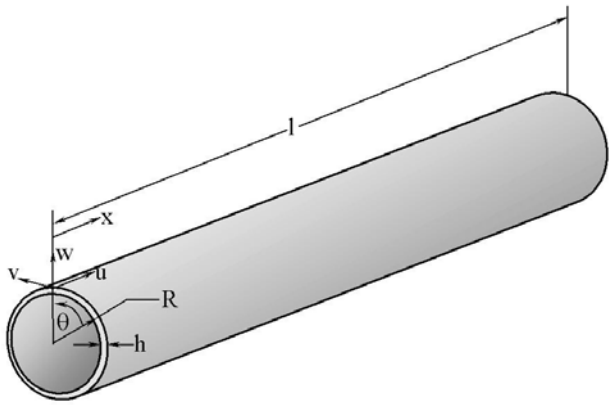

Figure 1: coordinate system of a thin circular cylindrical shell (from Ref [1]).

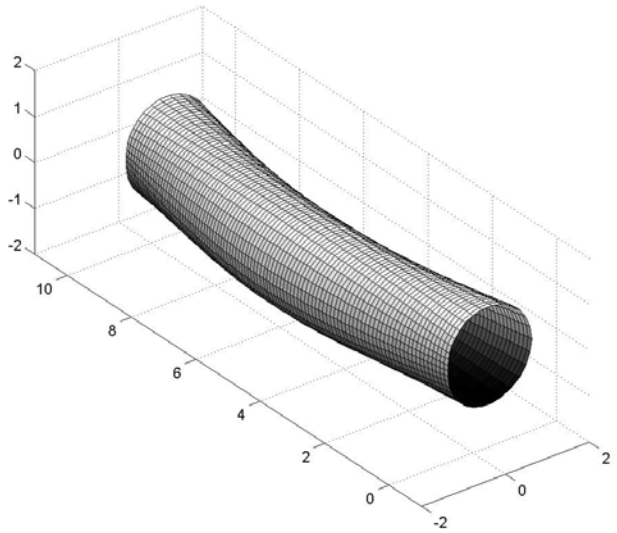

Figure 2: first bending mode from thin shell theory: (1,1).

EXPERIMENTAL APPROACH

Once the mode shapes were determined for the circular cylindrical shell, a series of experiments were performed to determine the effects on modal stiffness, mass, and damping that the cardboard liner has on the shell system. The effects were determined by tracking the changes in frequency for each mode when the cardboard insert is introduced into the system.

An aluminum shell was used in the experiments with the following geometry: R/h=31.25, l/R=16.4, and h=2.032 mm. To remain consistent with the mode shapes developed in the previous section, hanging each end of the shell by elastic cords simulated the free-free boundary condition. The low stiffness of the cords ensured that rigid body bounce modes well below the frequencies of interest in the shell.

For the two test conditions, accelerometers were placed in five equally spaced positions along the shell in the longitudinal (x) direction. In order to detect repeated roots arising from the symmetric geometry of the shell, a second row of accelerometers was placed orthogonal to the original row. A microphone was also

placed in the vicinity of the shell to document the effects on acoustic radiation from the addition of the cardboard insert.

An impact hammer excited the shell. The impact locations were at each end of the shell and in both horizontal and vertical directions, aligning with the directions of the accelerometers. The multiple excitation points were collected to ensure that the repeated roots of the symmetric structure were detected through populating multiple rows of the FRF matrix. The locations of the excitation and response locations are shown in figure 3.

From the experiment, accelerance, and acoustic sensitivity FRFs were calculated for each excitation and response location. Commercial modal analysis software was used to curve fit the FRFs to obtain the natural frequencies, damping ratios, and modal vectors. Due to the relatively light amount of damping in the system and the multiple excitation locations, the time domain multiple degree of freedom (MDOF) excitation model was chosen for curve fitting.

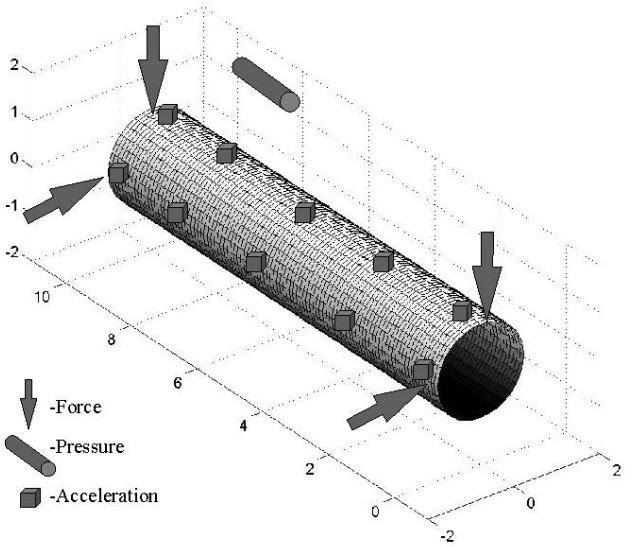

Figure 3: Excitation and response locations on the shell.

RESULTS

Figure 4 displays a driving point accelerance FRF and an acoustic sensitivity FRF for the cases with and without the cardboard liner. Table 1 summarizes the modal parameters obtained by curve fitting the accelerance FRFs and comparing the mode shapes generated at each resonant frequency to the thin shell forms. It is seen from figure 4 that the modal behavior is significantly altered when the liner is introduced. Inspection of the table reveals that generally the cardboard liner increases the modal stiffness and adds modal damping to the system. Contrasting this observation, the (1,2) "shell" type mode experienced a decrease in the natural frequency and damping ratio, implying that increase in the modal mass was the dominant effect. It may also be noticed from the figure that the acoustic radiation of all of the modes was significantly reduced except for this (1,2) mode. Therefore, it may be stated that generally the liner adds stiffness and damping to the shell system, and thus reduces the generation of sound into the field. However, there may be special cases were some modes are more affected by the modal mass than stiffness, and the resonant behavior is not attenuated. This observed effect is not unique in propeller shaft liner applications.

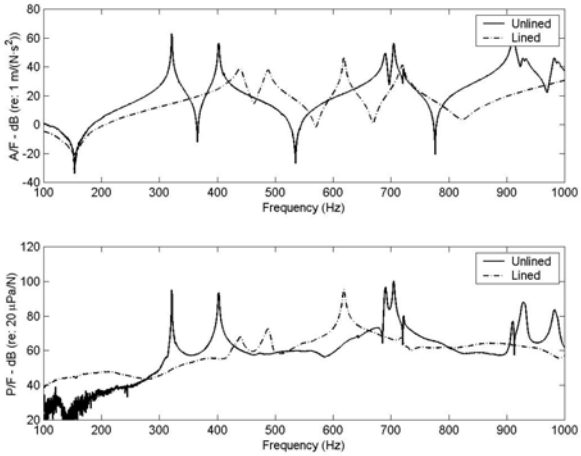

Figure 4: driving point FRFs at one end of the shell for the unlined and cardboard lined cases. Top: accelerance. Bottom: acoustic sensitivity.

Table 1: estimated natural frequencies and damping ratios for the unlined and cardboard lined shell. *

Mode Shape	Unlined Shell f_n (Hz)	ζ (%)	Cardboard Lined Shell f_n (Hz)	ζ (%)
Love mode, n=1	321	0.09	422	1.15
(1,1)	402	0.13	486	0.84
(1,2)	690	0.32	618	0.22
(2,1)	704	0.25	718	0.55
(2,2)	721	0.03	1258	1.00

*Repeated roots not shown

COULOMB FRICTION DAMPING

Table 1, which summarized the modal behavior of the shell, reveals that generally the cardboard liner increases the modal stiffness and modal damping in the system. The appropriate model that provides this increase in modal damping is often assumed to be Coulomb friction damping, *a priori*. The purpose of this section is to present the results of a study conducted to determine if the modal damping provided by the cardboard liner is indeed best modeled by Coulomb friction damping.

CHARACTERISTICS OF COULOMB FRICTION DAMPING

Coulomb friction damping is characterized by a constant damping force opposing the harmonic motion of the system. This force is proportional to the coefficient of friction between the two surfaces. The implication of this external force is that the decay envelope of free vibration is linear, rather than an exponential envelope found from other models such as viscous and hysteretic damping. Various sources in the literature address this phenomenon. In particular, Ref [2] shows that the decrement in amplitude per cycle is constant in the presence of friction and can be represented as:

$$\Delta x = x_{n+1} - x_n = 4\frac{F}{k} \tag{5}$$

This result assumes a constant damping force in a single degree of freedom system. Here x_n is the free vibration amplitude of the nth cycle, F is the external damping force, and k is the stiffness. Further, it is shown in Ref [2] for viscous damping that:

$$x_{n+1} = x_n e^{\delta} \Rightarrow \ln\left(\frac{x_{n+1}}{x_n}\right) = \delta \tag{6}$$

Here, δ is the logarithmic decrement for small damping. Note that the amplitude of vibration in (5) decreases in equal amounts as an arithmetic series and produces a linear decay envelope. The result is obviously different for (6) where the amplitude is shown to decrease in equal *percentage* amounts as a geometric series and produces an exponential decay envelope.

EXPERIMENTAL APPROACH

In order to confirm or contradict the presence of Coulomb friction damping on a modal basis, the time domain free response of the system is needed at a particular resonant frequency. The free response is found after being subjected to an initial excitation at that resonant frequency. Therefore, acceleration responses of the shell were collected using the same experimental approach for finding the FRFs described earlier in the report. In this case, propeller shaft attachment yokes were included in the experiment to represent a realistic propeller shaft response. The yokes also added large end-masses to the system and changed some of the mode types to a fixed-fixed type of boundary condition. This boundary condition constrained the motion at the attachment points for the elastic cords on each end, and consequently, the external damping provided to the system by these cords was minimized.

FILTER DESIGN

Although an impact hammer excites a broad range of frequencies, the response of a single mode can be found by attenuating the time domain results outside of a particular resonant frequency band through digital filtering. Therefore, the acceleration responses in the time domain were measured and a FFT into the frequency domain was performed on these responses. The filter was designed according to the identified resonant frequencies of the system found from the FFT.

The Elliptic (or Cauer) filter design was used to capture the acceleration response of a singe mode. This Infinite Impulse Response (IIR) filter was chosen based on the characteristics given in Ref [4]:

1. The Elliptic filter yields a sharper cutoff frequency in comparison to other designs such as Chebyshev and Butterworth.
2. The equiripple in the pass band and stop band is the best that can be achieved in comparison to other filter designs for a given filter order.
3. The IIR filter design has closed form design formulas, and as a result is more computationally efficient than the Finite Impulse Response (FIR) designs.

However, a disadvantage of IIR filters is that they exhibit non-linear phase around the transition regions between the pass band and stop bands. To correct for the phase distortion, the filtered signal can be inverted and re-filtered, thus reversing the effects of the phase distortion on the signal. This inversion process also has the advantage of further attenuating the signal outside the pass band when the filter is applied a second time.

Table 2 summarizes the lower and upper bounds chosen to isolate each resonant frequency for the fourth order Elliptic filter used in the study. An example of the filter frequency response is shown in figure 5, where sharp transition regions and minimized equiripple in both the pass and stop bands are present, as expected.

Table 2: lower and upper cutoff frequencies for the digital filter.

f_n (Hz)	Lower Bound (Hz)	Upper Bound (Hz)
394	320	400
424	405	435
447	435	460
528	480	625
708	650	850

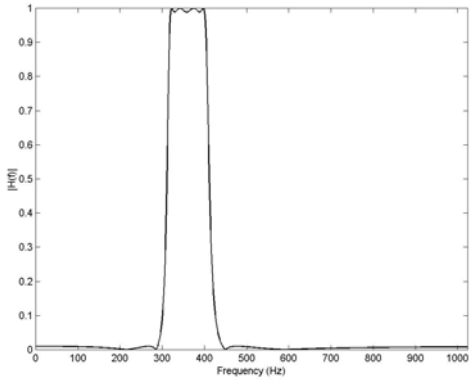

Figure 5: frequency response of a fourth order Elliptic IIR filter with the pass band between 320 and 400 Hz.

RESULTS AND DISCUSSION

Figure 6 displays the unfiltered and filtered acceleration amplitude, phase, and the filtered time domain acceleration response. Inspection of c) shows that the response is dominated by an exponentially decaying envelope rather than a linearly decaying envelope. Therefore, it may be concluded that Coulomb friction is not the appropriate damping model for the cardboard insert-shell structure for this mode. It may also be noted from a) and b) in Figure 6 that signal outside the pass band of the filter is well attenuated with negligible phase distortion. Results for the other resonant modes are shown in the appendix. The same conclusions may be drawn in all cases.

The conclusion that Coulomb friction is not an appropriate damping model is an interesting result. It has been found in many propeller shaft applications that the cardboard liner tends to disintegrate over time; dust particles are often found in the inside of the shaft after many cycles. Such an observation would lead one to conclude that friction is present in the liner-propeller shaft system. However, from this analysis it has been shown that the friction is not significant as a vibration damping mechanism. A more appropriate damping model is investigated further in the next section.

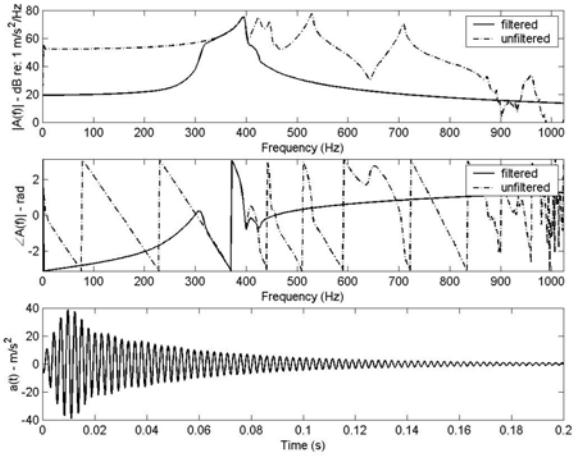

Figure 6: a) frequency domain acceleration amplitude response, b) frequency domain acceleration phase response, c) corresponding filtered time domain acceleration response for the digital filter pass band between 320 and 400 Hz.

VISCOUS DAMPING

It was shown in the previous section that Coulomb friction damping is not an appropriate model for a cardboard liner in a thin shell structure. Therefore, an analysis to determine the appropriate model by a second approach is presented in this section. Specifically, the hypothesis regarding viscous damping as the appropriate damping model is analyzed.

CHARACTERISTICS OF VISCOUS DAMPING

Ref [4] presents a method for determining the damping mechanism in a system by using estimated complex natural frequencies and mode shapes from a set of experimentally determined transfer functions. It is shown in the reference that the imaginary parts of the natural frequencies are responsible for the diagonal terms of the damping matrix (in physical coordinates) and the imaginary parts of the mode vectors are responsible for the off-diagonal terms. The real parts of the complex natural frequencies and modes are the same as the undamped natural frequencies and modes, respectively. To obtain these results, it is assumed that the damping in the system is light so that a first order perturbation method for determining complex natural frequencies and mode shapes is a sufficiently accurate procedure. By constructing the damping matrix in this manner, the reference shows by example that if “a non-symmetric damping matrix is obtained then it may be deduced that the physical law behind the damping mechanism in the structure is not viscous.” The procedure outlined in Ref [4] is restated in the appendix for convenience.

RESULTS

By using the transfer functions obtained earlier in the study, the damping matrix of the unlined shell as a function of the measured degrees of freedom is shown in figure 7. Figure 8 displays the matrix for the cardboard lined shell. In both cases, the matrices are symmetric implying that viscous damping is an appropriate damping model to represent the damping in the system. Indeed, when comparing the unlined matrix to the lined matrix, the diagonal terms of the lined matrix become more pronounced than the unlined matrix. One may deduce from this increased dominance of the diagonal terms that there is an increase in proportional viscous damping when the cardboard liner is present.

Further inspection of the matrices reveals that the amplitudes of viscous damping are obviously incorrect. The errors are thought to arise from the difficulty in normalizing complex modal vectors. Consequently, the matrix may not directly be used in lumped parameter and finite-element methods for calculation of transfer functions. Nevertheless, the symmetric nature of the matrices, and the increased dominance of the diagonal terms in the cardboard lined matrix, are still interesting results. The implication of such results is that the damping ratios obtained from an experiment can be used in finite-element-calculations as proportional viscous damping on a mode-by-mode basis with greater confidence for the damping model. The causes of the amplitude errors obtained in the damping matrices are the subject of further study.

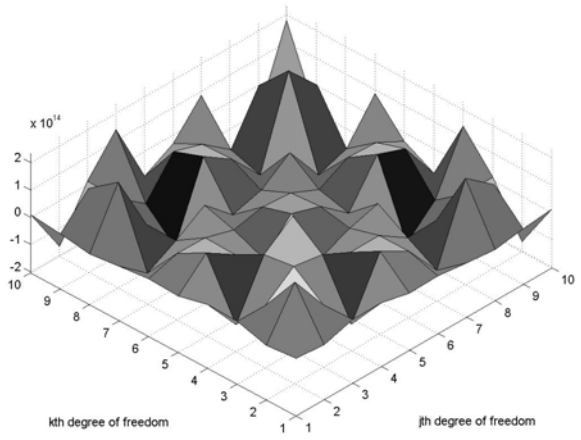

Figure 7: damping matrix for the unlined shell case.

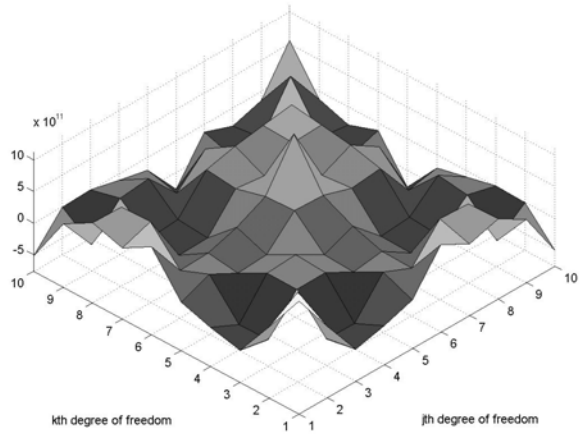

Figure 8: damping matrix for the cardboard lined shell case.

CONCLUSION

It has been shown in the study that the application of a cardboard liner to a thin circular-cylindrical shell significantly changes the modal behavior of the shell. The liner adds modal stiffness to most of the modes in the system, while an increase modal mass is also an observed effect for a certain shell type mode.

It has also been shown that the liner adds damping to the same modes where an increase in stiffness was the observed effect. Through inspection of the free vibration decay envelope, it was shown that Coulomb friction is not an appropriate damping model for a cardboard liner. Further, by construction and inspection of the damping matrix from experimentally determined complex natural frequencies and modal vectors, it was found that proportional viscous damping appears to be an appropriate damping model.

Because proportional viscous damping was found to be an appropriate model for the cardboard liner, experimentally determined modal damping ratios may be used in lumped parameter and finite-element calculations with a greater degree of confidence. Because of the results obtained in this study, the analytical tools may be more effectively used to analyze thin shell structures such as propeller shafts and the need for costly trial-and-error hardware testing is reduced.

ACKNOWLEDGMENTS

The first author would like to thank Mark Gehringer for suggesting work on the project. In addition, thanks to Pam Nielsen for assistance with the project. The first author would also like to recognize Dr. Jim De Clerck and Dr. Rajendra Singh for technical guidance. Finally, thanks to Dr. Jim Woodhouse for help in understanding his paper on the damping matrix.

REFERENCES

1. Leissa, Arthur. Vibration of Shells. The Acoustical Society of America, 1993.
2. Den Hartog, J. P. Mechanical Vibrations. New York: Dover Publications, Inc. 1985.
3. Oppenheim, Alan V. and Ronald W. Schafer. Digital Signal Processing. New Jersey: Prentice-Hall Inc., 1975.
4. Adhikari, S. and J. Woodhouse. "Identification of Damping: Part 1, Viscous Damping." *J. Sound and Vib.* (2001) **243**(1), 43-61.
5. Matlab, Student Version 5.3.0. "Online help files."
6. Email discussion with Dr. James Woodhouse, May 2002.
7. Discussions with Dr. Rajendra Singh, September 2001 – June 2002.

CONTACT

Martin G. Foulkes is a Noise and Vibration project engineer at General Motors Corporation. He may be contacted at: martin.g.foulkes@gm.com.

James P. De Clerck is a project leader for structural vibration and vibration methods at General Motors Corporation. He may be contacted at: james.p.declerck@gm.com.

Rajendra Singh is the Donald D. Glower Chair and Professor of Mechanical Engineering at the Ohio State University. He may be contacted at: singh.3@osu.edu.

APPENDIX

A. DETERMINATION OF THE DAMPING MATRIX

The method for constructing the damping matrix from complex natural frequencies and modal vectors in Ref [5] is restated here for convenience.

1. Measure a set of transfer functions $H_{ij}(\omega)$.
2. Choose the number m of modes to be retained in the study. Determine the complex natural frequencies $\hat{\lambda}_j$ and complex mode shapes $\hat{z}_j$ form the transfer functions, for all $j = 1 \ldots m$. Obtain the complex mode shape matrix $\hat{Z} = [z_1, z_2, ..., z_m] \in C^{N \times m}$.
3. Estimate the "undamped natural frequencies" as $\omega_j = \Re(\hat{\lambda}_j)$.
4. Set $\hat{U} = \Re[\hat{Z}]$ and $\hat{V} = \Im[\hat{Z}]$, and from these obtain $W = \hat{U}^T \hat{U}$ and $S = \hat{U}^T \hat{V}$. Now denote $B = W^{-1} S$.
5. From the B matrix get $C'_{kj} = (\hat{\omega}_j^2 - \hat{\omega}_k^2) B_{jk} / \hat{\omega}_j$ for $k \neq j$ and $C'_{jj} = 2\Im(\hat{\lambda}_j)$.
6. Finally, carry out the transformation $C = \left[\left(\hat{U}^T \hat{U}\right)^{-1} \hat{U}^T\right]^T C' \left[\left(\hat{U}^T \hat{U}\right)^{-1} \hat{U}^T\right]$ to get the damping matrix in physical coordinates.

ADDITIONAL RESULTS

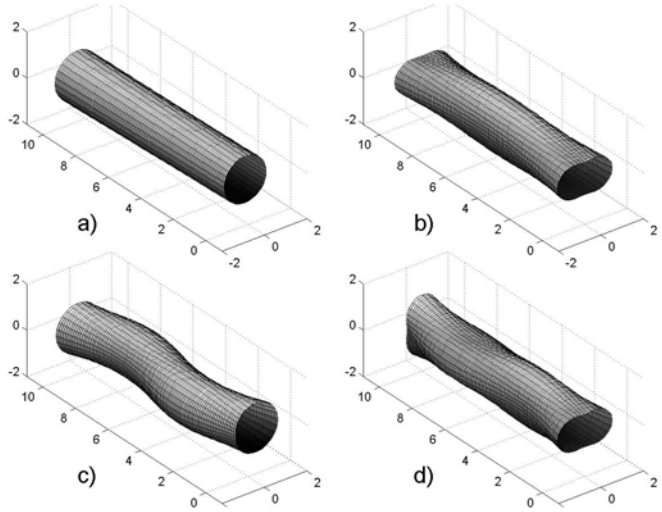

Figure 9: calculated mode shapes from thin shell theory: a) Love Mode n=1, b) Shell mode (1,2), c) Bending Mode (2,1), d) Shell Mode (2,2).

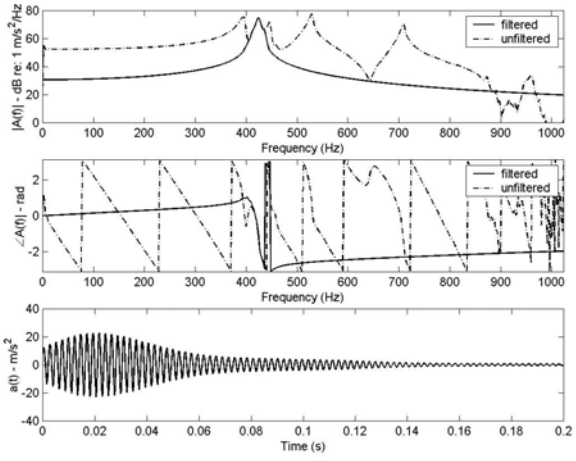

Figure 10: a) frequency domain acceleration amplitude response, b) frequency domain acceleration phase response, c) corresponding filtered time domain acceleration response for the digital filter pass band between 405 and 435 Hz.

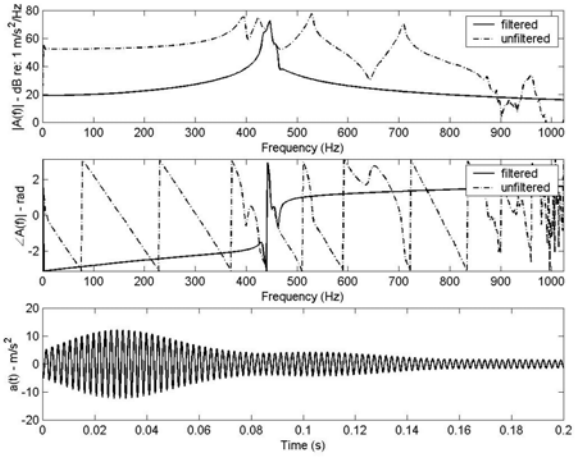

Figure 11: a) frequency domain acceleration amplitude response, b) frequency domain acceleration phase response, c) corresponding filtered time domain acceleration response for the digital filter pass band between 435 and 460 Hz.

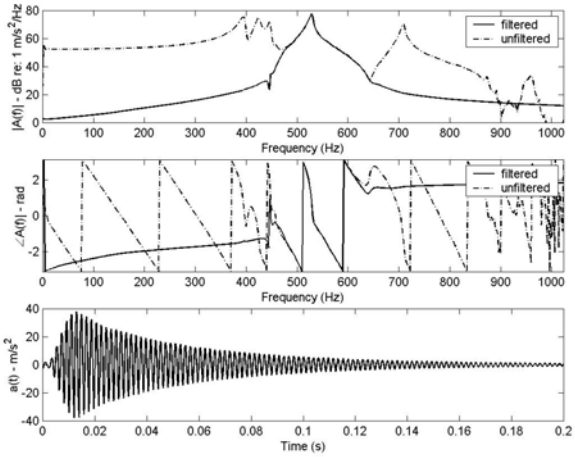

Figure 12: a) frequency domain acceleration amplitude response, b) frequency domain acceleration phase response, c) corresponding filtered time domain acceleration response for the digital filter pass band between 480 and 625 Hz.

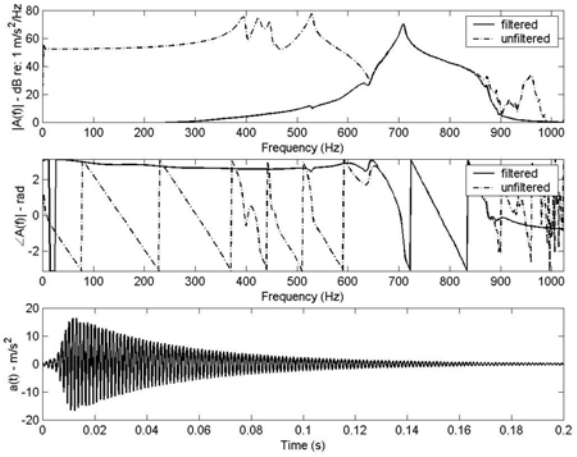

Figure 13: a) frequency domain acceleration amplitude response, b) frequency domain acceleration phase response, c) corresponding filtered time domain acceleration response for the digital filter pass band between 650 and 850 Hz.